Mutations in the RNA Granule Component TDRD7 Cause Cataract and Glaucoma

Salil A. Lachke,[1]* Fowzan S. Alkuraya,[1,2,3,4]* Stephen C. Kneeland,[5]* Takbum Ohn,[6]†
Anton Aboukhalil,[1,7] Gareth R. Howell,[5] Irfan Saadi,[1]‡ Resy Cavallesco,[1] Yingzi Yue,[1]
Anne C-H. Tsai,[8] K. Saidas Nair,[5] Mihai I. Cosma,[5,9] Richard S. Smith,[5] Emily Hodges,[10]
Suad M. AlFadhli,[11] Amal Al-Hajeri,[11] Hanan E. Shamseldin,[2] AbdulMutalib Behbehani,[12]
Gregory J. Hannon,[10] Martha L. Bulyk,[1,13,14] Arlene V. Drack,[15] Paul J. Anderson,[6]
Simon W. M. John,[5,16]§ Richard L. Maas[1]§

The precise transcriptional regulation of gene expression is essential for vertebrate development, but the role of posttranscriptional regulatory mechanisms is less clear. Cytoplasmic RNA granules (RGs) function in the posttranscriptional control of gene expression, but the extent of RG involvement in organogenesis is unknown. We describe two human cases of pediatric cataract with loss-of-function mutations in *TDRD7* and demonstrate that *Tdrd7* nullizygosity in mouse causes cataracts, as well as glaucoma and an arrest in spermatogenesis. TDRD7 is a Tudor domain RNA binding protein that is expressed in lens fiber cells in distinct TDRD7-RGs that interact with STAU1-ribonucleoproteins (RNPs). TDRD7 coimmunoprecipitates with specific lens messenger RNAs (mRNAs) and is required for the posttranscriptional control of mRNAs that are critical to normal lens development and to RG function. These findings demonstrate a role for RGs in vertebrate organogenesis.

I n eukaryotic cells, cytoplasmic RNA granules (RGs) function in determining whether mRNAs undergo degradation, stabilization, or intracellular localization (*1–3*). Lower eukaryotes such as yeast harbor RGs that are classified as either processing bodies (PBs) or stress granules (SGs) (*3, 4*), whereas metazoan cells harbor additional classes of RGs (*5–7*). Somatic cells contain both PBs and transport ribonucleoprotein (RNP) particles and accumulate SGs in response to environmental stress (*8, 9*). PBs contain components of mRNA decay processes like Xrn1-mediated 5′ to 3′ degradation, nonsense-mediated decay (NMD), and microRNA-mediated silencing, and serve as sites where mRNAs can be either stored or degraded (*10*). In neuronal cells and fibroblasts, RNPs function in the transport and localized translation of mRNAs involved in synapse formation or motility (*8, 11*). SGs store bulk mRNA during conditions of stress and can interact with PBs to exchange mRNAs that are then directed to translational reinitiation or degradation (*9, 12*). Lastly, germ cells contain germ cell–specific granules (GCG) that have been implicated in germ cell specification (*2, 7*).

Proteins with roles in development have been associated with RGs (*13*), but the importance of this association and that of somatic cell RGs in metazoan organogenesis remains unknown. For example, the precise spatial and temporal expression of key transcription factors is essential for normal transcriptional regulation during development. However, whether a similar level of developmental control exists over the expression of factors involved in posttranscriptional mRNA regulation, and whether this control is required for organogenesis, is unclear. We report the identification of Tudor domain–containing 7 protein, or TDRD7, as an RG component with a highly enriched and conserved pattern of developmental expression in the vertebrate ocular lens. In lens, we identify TDRD7 as a component of a unique class of RNPs and show that these TDRD7-RNA granules (TDRD7-RGs) differentially associate with lens PBs and RNPs that contain a known RG component, STAU1 (STAU1-RNPs). Furthermore, human *TDRD7* mutations result in cataract formation via the misregulation of specific, developmentally critical lens transcripts, and *Tdrd7* null mutant mice develop cataract as well as glaucoma, the latter defined by elevated intraocular pressure (IOP) and optic nerve damage.

The study of patients with balanced chromosomal rearrangements represents an important entry point to understanding disease mechanisms, and numerous examples exist of disease genes that have been identified by virtue of being disrupted by rearrangement breakpoints (*14*). As part of the Developmental Genome Anatomy Project (DGAP) (www.bwhpathology.org/dgap), we ascertained a male patient, designated DGAP186, with juvenile cataract and hypospadias who has a de novo balanced paracentric inversion of chromosome 9, 46,XY,inv(9)(q22.33q34.11) (Fig. 1, A and B).

We determined that the 9q34.11 breakpoint disrupts the gene *NR5A1* (fig. S1). *NR5A1* encodes a steroid nuclear receptor protein implicated in hypospadias in mouse and human mutants without cataract (*15–17*). *NR5A1* disruption is therefore likely to explain the reproductive tract phenotype and unlikely to account for the cataract phenotype in DGAP186. Analysis of the 9q22.33 breakpoint revealed that *TDRD7* is disrupted (Fig. 1, B and C, and fig. S1), and *TDRD7* haploinsufficiency as a direct result of the allelic disruption was observed in DGAP186 lymphoblastoid cells at both the RNA and protein levels, (Fig. 1D and fig. S1).

To independently confirm the involvement of *TDRD7* in pediatric cataract, we identified a family, F3R, with autosomal recessive congenital cataract. Homozygosity mapping (*18*) identified a single block of shared homozygosity between the four affected siblings that spanned the *TDRD7* locus (Fig. 1E and fig. S2). Furthermore, bidirectional sequencing of *TDRD7* uncovered a novel in-frame 3–base pair deletion that removes a highly conserved amino acid, V618 (Fig. 1F and fig. S2). This V618del variant, which was not detected in 320 ethnically matched controls (640 chromosomes), is predicted to disrupt the structure of TDRD7 and is therefore likely to represent a loss-of-function mutation (fig. S2).

To assay the endogenous expression of *TDRD7*, we turned to mouse and chick embryos. In situ hybridization revealed strong and highly specific expression of *Tdrd7* transcripts in the developing mouse lens (Fig. 2A and fig. S3). At embryonic day E12.5, *Tdrd7* is expressed in differentiating fiber cells in the posterior lens, whereas the anterior epithelium of the lens (AEL) lacks detectable expression. Expression of chick *TDRD7* is also high in the developing lens (Fig. 2B). To confirm a direct causal link between *TDRD7* haploinsufficiency and cataract formation, we used a replication-competent avian sarcoma (RCAS) viral vector (*19*) to deliver short hairpins that

[1]Division of Genetics, Department of Medicine, Brigham and Women's Hospital and Harvard Medical School, Boston, MA 02115, USA. [2]Department of Genetics, King Faisal Specialist Hospital and Research Center, Riyadh, 11211, KSA. [3]Department of Anatomy and Cell Biology, College of Medicine, Alfaisal University, Riyadh 11533, KSA. [4]Department of Pediatrics, King Khalid University Hospital and College of Medicine, King Saud University, Riyadh 11461, KSA. [5]Howard Hughes Medical Institute and The Jackson Laboratory, 600 Main Street, Bar Harbor, ME 04609, USA. [6]Division of Rheumatology, Immunology and Allergy, Department of Medicine, Brigham and Women's Hospital and Harvard Medical School, Boston, MA 02115, USA. [7]Department of Aeronautics and Astronautics, Massachusetts Institute of Technology, Cambridge, MA 02139, USA. [8]Department of Pediatrics, University of Colorado-Denver, Aurora, MA 00045, USA. [9]Department of Medicine, Maine Medical Center, Portland, Maine, ME 04102, USA. [10]Cold Spring Harbor Laboratory, Watson School of Biological Sciences and Howard Hughes Medical Institute, Cold Spring Harbor, NY 11724, USA. [11]Medical Laboratory Medicine, Faculty of Allied Health Sciences, Kuwait University, Kuwait City 13060, KW. [12]Department of Surgery, Faculty of Medicine, Kuwait University, Alsafat 13110, KW. [13]Department of Pathology, Brigham and Women's Hospital and Harvard Medical School, Boston, MA 02115, USA. [14]Harvard-Massachusetts Institute of Technology Division of Health Sciences and Technology (HST), Harvard Medical School, Boston, MA 02115, USA. [15]Department of Ophthalmology and Visual Sciences, University of Iowa, Iowa City, IA 52242, USA. [16]Department of Ophthalmology, Tufts University School of Medicine, Boston, MA 02115 USA.

*These authors contributed equally to this work.
†Present address: Division of Natural Sciences, Chosun University, Gwangju 501-759, South Korea.
‡Present address: Center for Regenerative and Developmental Biology, The Forsyth Institute, Cambridge, MA 02142, USA.
§To whom correspondence should be addressed. E-mail: maas@genetics.med.harvard.edu (R.L.M.); simon.john@jax.org (S.W.M.J.)

specifically targeted chick *TDRD7* to achieve RNA interference–mediated gene knockdown. *TDRD7*-knockdown short hairpin–mediated RNA interference (shRNA) retroviruses were injected in E2 [Hamburger and Hamilton stage 11 (HH st. 11)] optic vesicles, and the embryos were analyzed for the presence of cataract at E16 (HH st. 42). Injections of green fluorescent protein–expressing control RCAS virus led to highly efficient uptake by lens cells (fig. S3). At E16, a cataract phenotype was observed at significant frequency (17/115, 15%) in chick embryos injected with *TDRD7*-shRNA RCAS virus but not in those that received control virus (1/48, 2%; $P < 0.05$) (Fig. 2C and fig. S3). Quantitative reverse transcription polymerase chain reaction (qRT-PCR) analysis indicated that cataract formation was observed in lenses in which *TDRD7* transcripts were reduced to approximately 40% or less of control levels (fig. S3).

To gain further insight into TDRD7 function, we analyzed mutant mice with an N-ethyl-N-nitrosourea (ENU)–induced recessive mutation in *Tdrd7*. These mice, identified during a screen for glaucoma phenotypes, develop cataracts and high IOP. A nonsense mutation c.2187C>T (Q723X) produces a *Tdrd7* null allele, as determined by the absence of TDRD7 protein in homozygous mutants (fig. S4). Within 4 weeks of birth, all *Tdrd7* homozygous mutants developed a posterior cataract that became severe with age (Fig. 2, D and E). At later stages, the lens fiber cell compartment developed vacuoles with lens capsule rupture and extrusion of fiber cell mass into the vitreous (Fig. 2, F and G). This feature of the mouse lens phenotype precisely recapitulates the unusual posterior lenticonus (a conical projection of the lens surface) and posterior capsule defects observed in the DGAP186 proband (*15*). In addition, in some *Tdrd7* mutant mice, the mass of fiber cells passed through the pupil into the anterior chamber of the eye (fig. S4). By 4 months of age, iris flattening was detected and anterior chamber depth increased (fig. S5). By 6 months of age, the IOP was elevated in some *Tdrd7* mutants, and the incidence of elevated IOP increased with age (Fig. 2H and fig. S5). The ocular drainage structures Schlemm's canal and the trabecular meshwork normally influence IOP and are located in the angle of the anterior chamber—the angle formed between the iris and the cornea, where the aqueous humor flows out of the anterior chamber. If the egress of aqueous humor is impeded, the accumulated fluid leads to increased IOP, which in turn contributes to retinal ganglion cell (RGC) death and optic nerve atrophy, all of which are hallmarks of glaucoma. In *Tdrd7* mutants, the angles are largely normal in morphology with an open-angle configuration, defined by absence of morphologic obstruction (Fig. 2, I and J); the open-angle configuration also predominates in human glaucoma. In *Tdrd7* mutant mice, severe optic nerve atrophy characterized by RGC axon loss and excavative remodeling of the optic nerve were observed (Fig. 2, K to N, and fig. S5). Notably, in family F3R, two of the four

affected individuals developed glaucoma with open angles and increased IOP after cataract extraction, pointing to the *Tdrd7* mutant mouse as a potential model for certain aspects of human glaucoma.

TDRD7 contains five conserved Tudor class domains and three OST-HTH (Oskar-TDRD7-Helix-Turn-Helix)/LOTUS domains (Fig. 1B), which bind methylated arginine residues and RNA, respectively (*20*). TDRD1, TDRD6, and TDRD7 have been associated with a GCG known as the chromatoid body (CB) that is found in mammalian male germ cells (*21, 22*). To gain insight into TDRD7's cellular function, we generated a mouse TDRD7 antibody and analyzed protein expression during mouse embryogenesis. TDRD7 expression between E11.0 and E12.5 becomes markedly enriched in lens fiber cells, where it is expressed in numerous cytoplasmic granules of 0.3 to 0.8 μm diameter (Fig. 3, A and B, and fig. S6). A similar pattern was observed with a second independent TDRD7 antibody (fig. S6). TDRD7 granules were also found in differentiating secondary fiber cells in postnatal day 1 (P1) lens (fig. S6). To determine whether these TDRD7 positive granules contained RNA, we stained mouse E12.5 lens sections with SYTO RNASelect or Pyronin Y, two RNA-specific stains (Fig. 3C and fig. S7). Co-staining with TDRD7 antibody revealed that TDRD7 granules colocalize with RNA in lens fiber cell cytoplasm, and thus constitute bona fide RGs, denoted TDRD7-RGs (Fig. 3, C to E).

To establish whether TDRD7 is associated with a specific class of RGs in mouse embryonic lens, we examined the expression of protein markers for different classes of somatic cell RGs (*23*). Immunostaining of mouse embryonic lens sections with antibodies against the PB markers DCP1A and Ge-1 (*23*) demonstrated the presence of numerous cytoplasmic PBs in lens fiber cells (Fig. 3F and fig. S8). These structures were also found to contain DDX6/RCK and were dissociated by cycloheximide (CHX) (fig. S9), indicating that they are functional PBs. Costaining these sections with TDRD7 antibody demonstrated that TDRD7-RGs interact with PBs (Fig. 3F and fig. S8). In addition to colocalization, PBs and TDRD7-RGs were occasionally juxtaposed to each other,
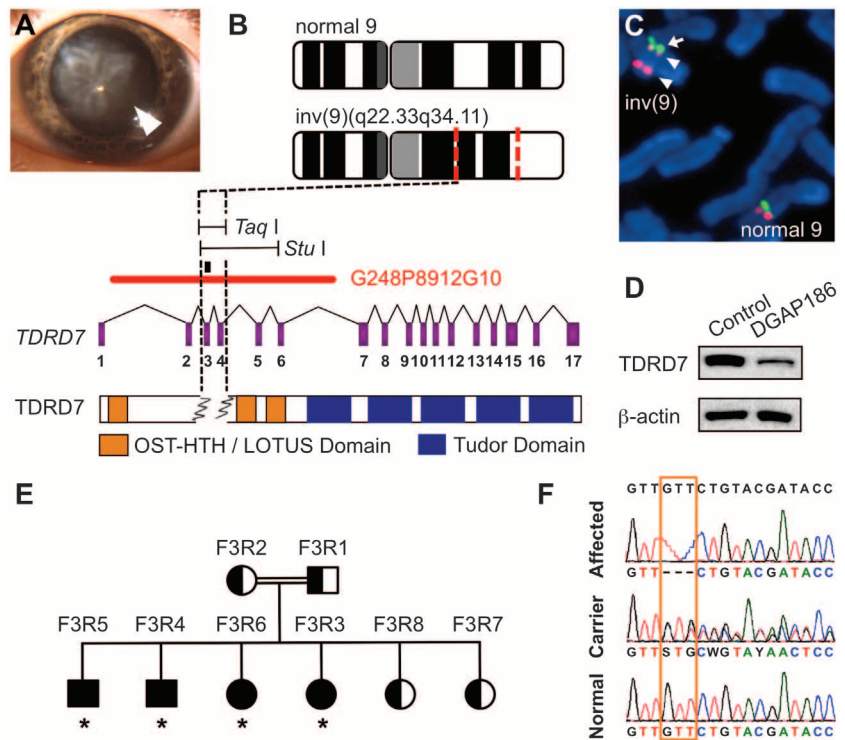
Fig. 1. *TDRD7* mutations in human pediatric cataract. (**A**) Cataract in DGAP186 (left eye, white arrowhead). (**B**) Ideogram of normal and inverted chromosome 9 [inv(9)]. Inversion breakpoints are shown by red lines, with a schematic below of *TDRD7*. Dotted black line marks breakpoint that disrupts *TDRD7* within the 2.6-kb region shown and in TDRD7 protein. The black bar indicates *TDRD7* genomic probe in Southern analysis. *Taq*I and *Stu*I refer to the fragments resulting from restriction enzyme digest. The red bar indicates fosmid clone G248P8912G10 used as a *TDRD7*-specific probe. Exons are indicated by purple boxes. (**C**) Chromosomal spread of DGAP186 lymphoblastoid cells analyzed by fluorescence in situ hybridization shows split *TDRD7*-specific red probe, whereas green anchor probe remains intact in inv(9). White arrowheads indicate inverted genomic region that hybridizes to *TDRD7*-specific probe; white arrow represents noninverted region (see fig. S1). (**D**) *TDRD7* haploinsufficiency is demonstrated by Western blot of DGAP186 lymphoblastoid cells. (**E**) Pedigree of consanguineous family F3R with congenital cataract (solid symbols, affected status; half-solid symbols, carrier status). (**F**) Sequence chromatogram shows c.1852_1854del (p.617delVal) mutation (boxed) in family F3R (see fig. S2).

in an arrangement similar to the docking-type interactions observed for DCP1A and STAU1-RNPs in neurons (fig. S8) (24). Quantification of both colocalizing and docking configurations between TDRD7 granules and PBs indicated a modest but significant degree of overall interaction [$12 \pm 4\%$, mean $\pm$ SEM, $n = 250$ PBs; $P < 1.5 \times 10^{-5}$, compared to a model of random distribution throughout the lens (15)].

STAU1 and STAU2, mammalian homologs of the *Drosophila* RNA-binding protein Staufen, are components of transport RNPs (25–27). Staining with STAU1 antibody revealed the presence of numerous STAU1-positive RNPs in lens fiber cells (Fig. 3G). These colocalized to a high degree ($29 \pm 5\%$, mean $\pm$ SEM, $n = 258$ granules)

with TDRD7 (Fig. 3G and fig. S10). Expression of TDRD7 and STAU1 proteins could be detected as early as E10.5 at the lens vesicle stage (fig. S10). When tested at E11.5, the extent of TDRD7-STAU1 colocalization was highest along the anterior edge of the elongating fiber cell compartment (Fig. 3H), which apposes the AEL at later developmental stages. Similar results were obtained with the second TDRD7 antibody (fig. S10). We also tested for other known components of RGs, namely TIA-1, TIAL1 (TIAR), STAU2, and HuR (ELAVL1) (23), and found that these were not components of mouse lens RGs at E12.5 (fig. S11).

Previous studies have indicated that RGs dynamically interact with each other, and they may

share components or participate in mRNA exchange (12). STAU1 is especially relevant, as it is a component of all four RG classes and functions in diverse aspects of RNA metabolism, including mRNA transport and mRNA decay (24, 28, 29). We therefore hypothesized that TDRD7 granules, either alone or through their interaction with STAU1-RNPs and PBs, might regulate the number of RGs in the cell as well as the expression levels of specific lens transcripts (fig. S12). We further postulated that the misregulation of specific mRNAs due to reduced *TDRD7* dosage might cause cataract formation. To test these hypotheses, we first performed *TDRD7* knockdowns in a U2OS cell line–based assay previously developed to identify genes critical for RG formation (13). These experiments revealed that *Tdrd7* knockdown led to significant reductions in the numbers of SGs and PBs (fig. S13). To determine whether this effect was conserved in lens cell lines with higher numbers of SGs and PBs, we examined the human lens cell line SRA01/04 and quantified the results. In these cells, *TDRD7*-knockdown produced a dramatic reduction in SGs, indicating that TDRD7 is critical for an appropriate response of these cells to stressful stimuli (Fig. 4A and fig. S14). In contrast, *TDRD7* knockdown produced only minimal effects on PB numbers. Statistically significant reductions in SG numbers were also observed in *Tdrd7*-knockdown experiments in a mouse lens–derived epithelial cell line, 21EM15 (henceforth *Tdrd7*-KD 21EM15) (30), where the reduction in *Tdrd7* expression of $60 \pm 4\%$ (mean $\pm$ SEM, $n = 3$) approximates that in DGAP186 lymphoblastoid cells due to haploinsufficiency (figs. S13 and S14).

Next, to identify *Tdrd7* deficiency–induced changes in gene expression, we performed microarray analyses in biological triplicate on *Tdrd7*-KD 21EM15 cells and compared the in vitro results to those obtained for *Tdrd7* null lenses. In initial microarray experiments, we observed that 21EM15 cells expressed 56 of the top 100 genes that are expressed during embryonic lens development, including *Tdrd7*. Thus, 21EM15 cells at least partly recapitulate the molecular events during endogenous lens development. In *Tdrd7*-KD 21EM15 cells, compared to 21EM15 cells infected with control vector, ~6% of expressed genes were differentially regulated at a threshold of a 1.3-fold or greater (table S1). Of particular interest, key genes that encode SG and PB components (*G3bp*, *Hspb1*, and *Ddx6*), mouse homologs of known human cataract genes (*Crygs* and *Epha2*), and genes involved in fiber cell differentiation (*Prox1*) were all significantly downregulated (Fig. 5A and fig. S15).

To extend these results in vivo, we further analyzed the *Tdrd7* null mouse lens. As expected from Western blot analyses (fig. S4), immunofluorescence confirmed a complete absence of TDRD7 in the lens (Fig. 4B). We then undertook a microarray expression analysis of isolated lenses from *Tdrd7* null mutants and littermate controls, focusing on postnatal days P4, three weeks before overt cataract appearance, and P30, when
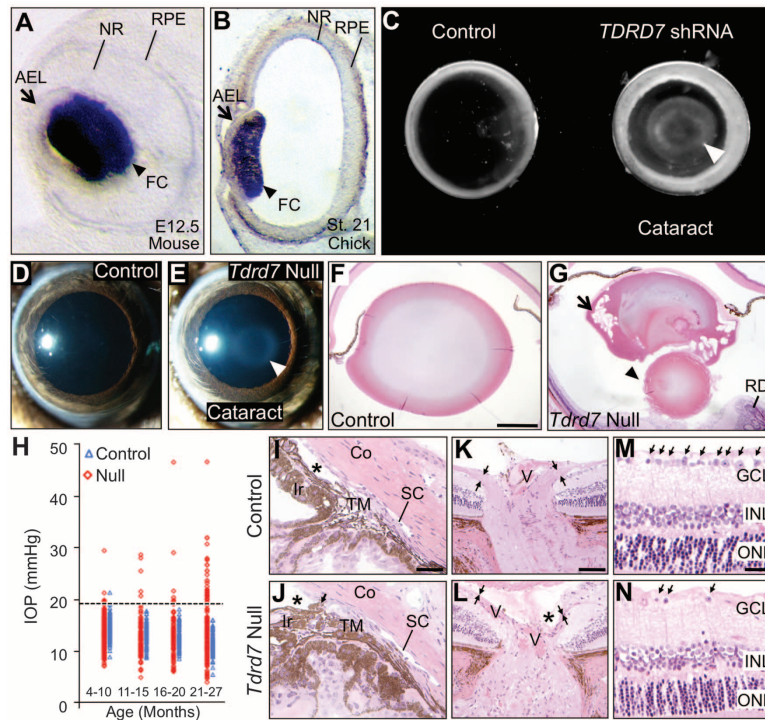
Fig. 2. *Tdrd7* deficiency causes cataract and glaucoma. (**A**) In situ hybridization of E12.5 mouse embryo (coronal section) demonstrates *Tdrd7* RNA expression in differentiating lens fiber cells (FC) (arrowhead), and its absence in the AEL (arrow). (**B**) In situ of stage 21 chick embryonic eye (coronal section) shows *TDRD7* expression in lens FCs (arrowhead) and absence in AEL. NR, neuroretina; RPE, retinal pigment epithelium. (**C**) Cataract (white arrowhead) in chick lenses infected with *TDRD7*-shRNA RCAS virus. (**D**) Absence of cataract in 1-month-old *Tdrd7* heterozygous mouse (control) and (**E**) cataract in age-matched *Tdrd7* null mouse lens. (**F**) Histology of control lens at 3 months shows no ocular abnormality and (**G**) a severe cataract in *Tdrd7* null mouse lens at same age. Note vacuoles in FC lens compartment (arrow) and rupture of lens capsule that extrudes fiber cell mass (arrowhead) into the vitreous. RD, mild to severe retinal dysplasia, focally present in some mutants. (**H**) *Tdrd7* null (red diamonds), but not control (blue triangles), mice exhibit age-dependent increase in IOP (see fig. S5). (**I** and **J**) Histology of iridocorneal angles showing normal morphology and open configuration (*) in both control (I) and mutant (J) eyes. Mutant angles are largely normal and open, but some mutants had mild, focal abnormalities of Schlemm's canal (SC) and trabecular meshwork (TM). Iris strands that attach to the cornea are common in mice (arrow) but are not continuous around the angle and do not block drainage. Angles of all histologically assessed mice with high IOP at 6 to 12 months were open ($n = 3$). Co, cornea; Ir, iris. (**K** to **N**) At ages >20 months, the optic nerve head and nerve fiber layer (RGC axons, arrows) in control mice (K) appear normal, whereas *Tdrd7* null mice (L) have considerable nerve damage with essentially no nerve fiber layer (arrows) and optic nerve head excavation (*). V, vessel. (**M** and **N**) Retinal periphery of control mouse (M) has normal cell density (arrows) in the ganglion cell layer (GCL), whereas mutant (N) with glaucomatous excavation of the nerve head has obvious cell loss. INL, inner nuclear layer; ONL, outer nuclear layer. Scale bars: [(F) and (G)] 500 μm; [(I) and (J)] 50 μm; [(K) and (L)] 100 μm; [(M) and (N)] 50 μm.

cataracts are fully penetrant. To accurately identify *Tdrd7*-dependent genes that function in lens development, we compared the P4 and P30 *Tdrd7* mutant mouse lens microarray data with that obtained from the *Tdrd7*-KD 21EM15 mouse lens cell line. Comparison of differentially regulated genes (DRGs) from the P4 and P30 *Tdrd7* null lens microarray data sets (each versus control), and the DRGs in *Tdrd7*-KD 21EM15 cells (versus control) identified several biologically relevant genes that were concordantly regulated in all three data sets (Fig. 5, A and B). These DRGs were classified into five distinct functional categories, denoted Classes I to V: Class I, genes involved in SG assembly or function; Class II, genes involved in P-body function and/or encoding helicases; Class III, genes linked to cataract or other ocular phenotypes; Class IV, crystallin genes (apart from Class III); and Class V, genes normally down-regulated during lens fiber cell differentiation (Fig. 5A). Whereas *Tdrd7* null lenses and *Tdrd7*-KD 21EM15 lens cells exhibit overlapping expression, each also exhibits unique categories of gene expression (e.g., Classes IV and V, respectively), and thus constitute complementary systems for revealing the full spectrum of DRGs attributable to *Tdrd7* loss-of-function.

Of 12 DRGs whose expression was significantly altered in *Tdrd7*-KD 21EM15 lens cells and that were relevant to lens development or RG function, six (*Hspb1, Ddx6, Ddx26, Epha2, Prox1,* and *Crygs*) were also concordantly down-regulated in *Tdrd7* null lens data sets. Two other genes that were down-regulated in both P4 and P30 *Tdrd7* null lenses, *Sparc* and *Crybb3*, are associated with cataracts and are thus also of interest (*31, 32*) (Fig. 5B). Thus, from comparative analyses of the microarray data, we identified eight genes that were significantly down-regulated in the *Tdrd7* null lens, *Tdrd7*-KD 21EM15 lens cells, or both, and that have biologically plausible links to lens development or RG function.

To determine whether the altered expression of these eight genes resulted from the direct or indirect action of TDRD7, we used qRT-PCR to confirm the microarray expression changes in P30 *Tdrd7* null lens RNA. This analysis confirmed the down-regulation of *Crybb3, Hspb1, Sparc,* and *Epha2* and of several other genes (fig. S15). We then performed RNA immunoprecipitation (RIP) experiments with TDRD7 antibody, followed by RNA isolation and RT-PCR. Because 21EM15 cells substantially recapitulate the expression profile of the developing lens, and there is considerable concordance in DRGs between the corresponding *Tdrd7* loss-of-function state, we employed 21EM15 lens cells for these experiments. *Crybb3* and *Hspb1* transcripts were markedly enriched in the TDRD7 immunoprecipitations, whereas *Epha2* transcripts were only modestly enriched and *Sparc* transcripts were not enriched (Fig. 5C). Thus, based on their strong *Tdrd7*-expression dependence and evidence for direct binding from the RIP experiments, we conclude that *Crybb3* and *Hspb1* mRNAs are

likely to be direct targets of TDRD7 regulatory function in the lens.

An attractive model emerges from these results. During lens development, AEL cells migrate into the lens "equatorial zone," where they differentiate into fiber cells. During fiber cell differentiation, because of the nuclear degradation process that helps promote lens clarity, most AEL-expressed genes cease transcription. By binding and stabilizing specific transcripts, TDRD7 and other RG components may facilitate the translation of crystallin mRNAs necessary to achieve the high protein levels and tight packing that provides for ocular transparency at high refractive index. TDRD7 also functions by maintaining mRNA expression levels of the heat shock gene *Hspb1*, which encodes a stress response chaperone protein that is a stress granule component that functions in mRNA decay (*33, 34*). Down-regulation of *Hspb1* mRNA levels is one of the earliest and quantitatively most striking gene expression changes we detect in *Tdrd7* null lenses.

HSPB1 down-regulation at the protein level was detected in P4 and P22 lenses (Fig. 4B and fig. S15). Interestingly, HSPB1 also interacts with several lens crystallin proteins (*35*) and stabilizes αB-crystallin (*36*). Moreover, destabilizing mutations in αB-crystallin are a known cause of congenital cataract (OMIM ID 123590). Thus, *Crybb3* and *Hspb1* are excellent candidates to contribute to cataract formation in *Tdrd7* loss-of-function mutants.

TDRD7 may also regulate certain transcripts indirectly. For example, TDRD7 deficiency results in reduction of *Sparc* transcripts, and *Sparc* null mice develop late-onset cataracts that resemble *Tdrd7* null mutant cataracts (*31*). These results place *Tdrd7* function upstream of *Sparc* mRNA expression and, because *Tdrd7* is involved in the regulation of multiple cataract genes (fig. S15), can explain the earlier cataract onset in *Tdrd7* mutants compared with *Sparc* mutants. In addition, *Sparc* and *Epha2* mRNAs have been described as direct targets of STAU1-RNPs, and
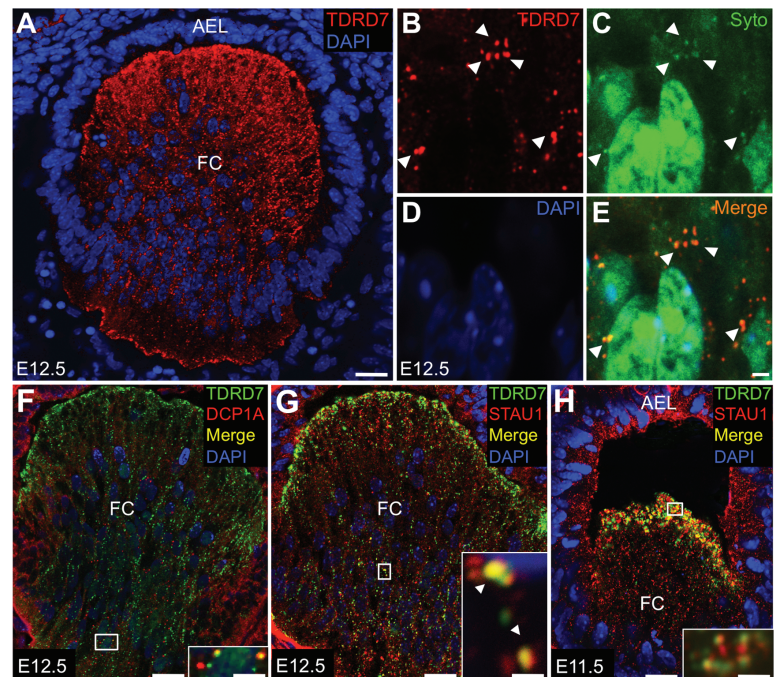
Fig. 3. TDRD7 RNA granules interact with STAU1-RNPs in lens fiber cells. (**A**) Immunofluorescence (IF) of mouse E12.5 lens (coronal section) with TDRD7 antibody demonstrates highly specific punctate expression in lens FCs and absence in AEL. (**B**) Higher magnification of E12.5 lens FCs stained with TDRD7 antibody shows numerous cytoplasmic granules (arrowheads). (**C**) Costaining with SYTO RNASelect reveals a similar pattern of cytoplasmic RNA granules (arrowheads). (**D**) 4′,6′-diamidino-2-phenylindole (DAPI) staining in same section. (**E**) Merged image [(B) to (D)] reveals colocalization (yellow) of TDRD7 with cytoplasmic RNA granules (see fig. S7). RNA staining of TDRD7 granules is somewhat variable and may reflect dynamic interactions of these granules. Scale bars: (A) 15 μm; (E) 2.5 μm. (**F**) IF of mouse E12.5 lens shows numerous cytoplasmic granules stained with antibodies against DCP1A (red) and TDRD7 (green). Colocalized granules appear yellow. (Inset) Higher magnification demonstrates colocalization of DCP1A P-bodies and TDRD7 RNA granules. (**G**) Staining of E12.5 lens with STAU1 antibody reveals numerous granules (red) in FC cytoplasm. These granules colocalize (yellow) to a high degree with TDRD7 granules (green). (Inset) Higher magnification indicates intimate colocalization (yellow, white arrowheads) of TDRD7 and STAU1 granules. (**H**) At E11.5, TDRD7 and STAU1 expression show a high degree of colocalization (yellow) in the anterior portion of the FC compartment. DAPI-stained nuclei are blue. (Inset) Higher magnification demonstrates high degree of colocalization (yellow) of TDRD7-RGs and STAU1-RNPs. Scale bars: (F) 15 μm; (F inset) 4 μm; (G) 15 μm; (G inset) 1 μm; (H) 10 μm; (H inset) 4 μm.

Epha2 mutations cause cataracts in both mouse and human (*26, 37*). Because STAU1-RNPs and TDRD7-RGs interact in the lens, *Sparc* and *Epha2* down-regulation in *Tdrd7* mutant lenses may reflect the disruption of this interaction between distinct RNPs and provide an additional mechanism of action for TDRD7 in the lens. A model encompassing both direct and indirect mechanisms of TDRD7 action in the developing lens is depicted in Fig. 5D.

In sum, TDRD7 is an RNA granule component that is highly enriched in the developing lens; TDRD7 perturbation in chick, mouse, and human causes cataract. In the lens, TDRD7-RGs play an essential role in the regulation of specific genes that are critical for lens development, including those responsive to stress, such as *Hspb1*. *Tdrd7* deficiency disturbs this regulatory mechanism and leads to cataract. The RNA granule function of TDRD7 may also be deployed in oth-

er tissues and cell types at various developmental stages. For example, TDRD7 is a component of a testis-specific RNA granule, the chromatoid body (CB) (*21*), and we observe that *Tdrd7* null mice exhibit male sterility due to an arrest in spermatogenesis at the round spermatid stage, likely due to a CB defect (fig. S16). Lastly, *Tdrd7* null mice develop elevated IOP and other features of glaucoma as they age. IOP elevation and glaucoma can result from oxidative and other stresses that

Fig. 4. *Tdrd7* is critical for RNA granule formation and HSPB1 expression. (**A**) SRA01/04 cell line shows increased numbers of P-bodies (detected by DDX6/RCK antibody) and stress granules (detected by elF3b antibody) in response to oxidative stress (sodium arsenite, 0.1 mM). The numbers of stress granules are markedly reduced, and P-bodies are modestly reduced in *TDRD7* knockdown SRA01/04 cells (for quantification, see fig. S14). Scale bar: 5 μm. (**B**) (Upper panels) IF with TDRD7 antibody demonstrates robust TDRD7-RGs in *Tdrd7* heterozygous mouse lens and absence in *Tdrd7* null mouse mutant lens. Scale bar: 3 μm. (Lower panels) IF with HSPB1 antibody demonstrates reduction of HSPB1 protein in P4 *Tdrd7* null lens (see fig. S15). Scale bar: 20 μm. EZ, equatorial zone; OFZ, organelle-free zone.
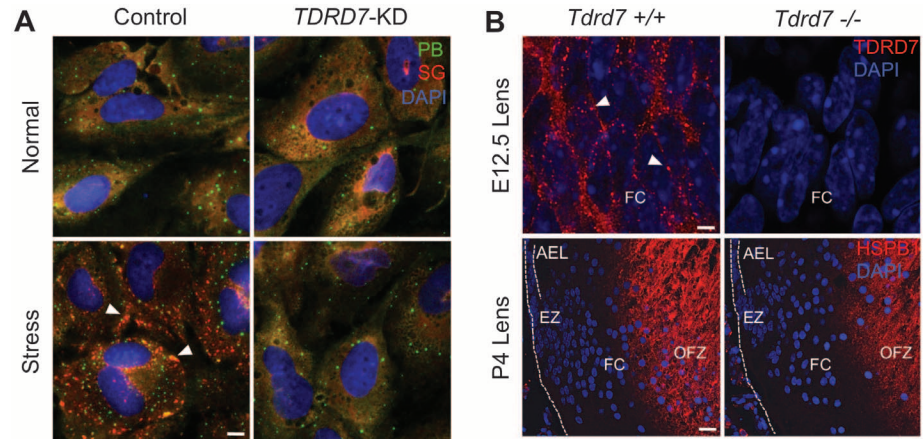
Fig. 5. TDRD7 regulates mRNAs critical to lens development and RG function. (**A**) Microarray analyses of *Tdrd7*-KD 21EM15 mouse lens cells reveals down-regulation of RNA granule genes and human cataract genes and up-regulation of other genes normally down-regulated during fiber cell differentiation. Genes are assigned to specific classes, denoted I to V. *Jag1* is expressed in fiber cells but is highly restricted. (**B**) Microarray analyses of mouse *Tdrd7* null mutant lens at P4 and P30 reveals down-regulation of RNA granule genes and human cataract genes. Fold changes (FC) are expressed as Log$_2$(FC). Error bars in (A) and (B) represent propagated SEM. (**C**) RIP using TDRD7 antibody, followed by RT-PCR, reveals *Crybb3*, *Hspb1* enriched in TDRD7 complexes. (**D**) Model for TDRD7 function in lens development. In lens fiber cells, TDRD7-RGs regulate certain key lens transcripts (e.g., *Crybb3* and *Hspb1*) directly via binding, and others indirectly via interactions with STAU1-NPs, which also bind specific transcripts (e.g., *Sparc* and *Epha2*) directly (*26*). These interactions may allow TDRD7, alone or in conjunction with STAU1, to protect specific mRNAs from the RNA decay mechanisms that exist in lens fiber cells, thus selectively stabilizing these mRNAs for translating the high levels of refractive proteins needed for lens transparency.
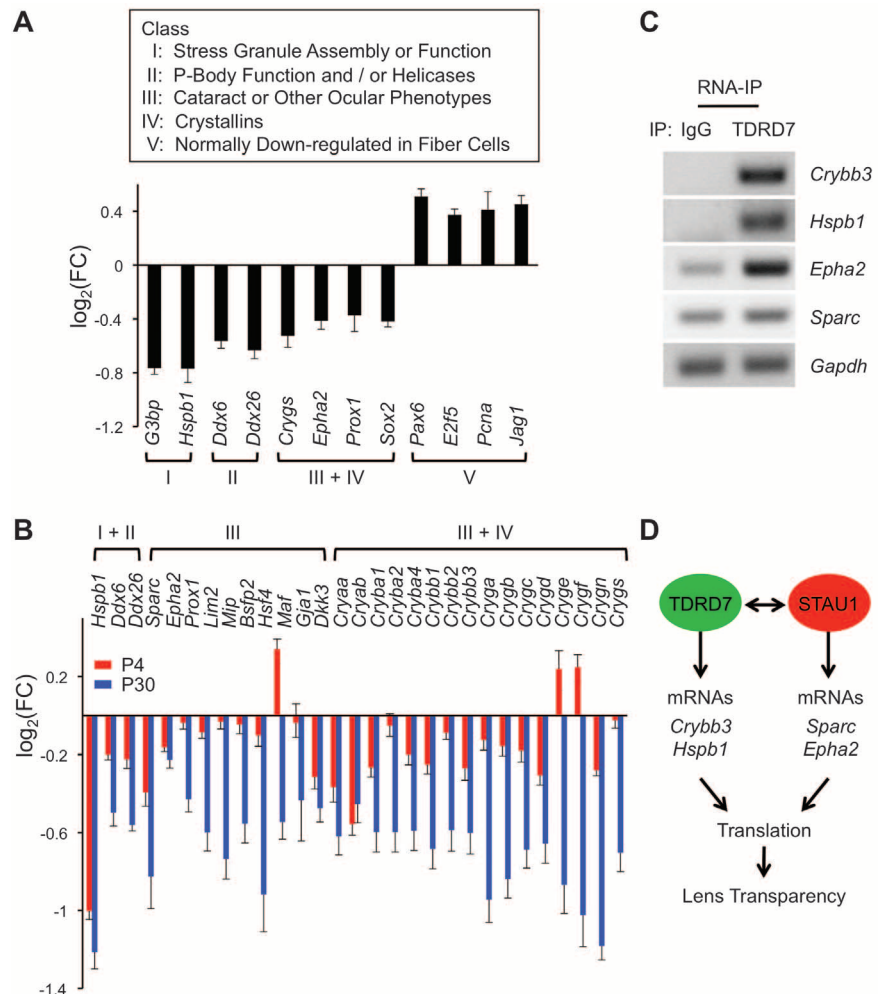
damage the aqueous humor drainage tissues (*38*). It is possible that the IOP elevation in *Tdrd7* null mice and in the two human patients who developed glaucoma results, at least in part, from abnormalities in the protective stress response or in other TDRD7-related functions in the drainage tissues. Thus, the data demonstrate that human organogenesis defects can result from perturbation of a distinct, tissue-specific RG component that posttranscriptionally regulates the levels of developmentally critical mRNAs.

References and Notes

1. M. J. Moore, *Science* **309**, 1514 (2005).
2. P. Anderson, N. Kedersha, *Nat. Rev. Mol. Cell Biol.* **10**, 430 (2009).
3. R. Parker, U. Sheth, *Mol. Cell* **25**, 635 (2007).
4. U. Sheth, R. Parker, *Science* **300**, 805 (2003).
5. S. Vasudevan, J. A. Steitz, *Cell* **128**, 1105 (2007).
6. A. Eulalio, I. Behm-Ansmant, E. Izaurralde, *Nat. Rev. Mol. Cell Biol.* **8**, 9 (2007).
7. N. Kotaja, P. Sassone-Corsi, *Nat. Rev. Mol. Cell Biol.* **8**, 85 (2007).
8. M. A. Kiebler, G. J. Bassell, *Neuron* **51**, 685 (2006).
9. J. R. Buchan, R. Parker, *Mol. Cell* **36**, 932 (2009).
10. M. Brengues, D. Teixeira, R. Parker, *Science* **310**, 486 (2005).
11. Y. Oleynikov, R. H. Singer, *Curr. Biol.* **13**, 199 (2003).
12. N. Kedersha et al., *J. Cell Biol.* **169**, 871 (2005).
13. T. Ohn, N. Kedersha, T. Hickman, S. Tisdale, P. Anderson, *Nat. Cell Biol.* **10**, 1224 (2008).
14. A. W. Higgins et al., *Am. J. Hum. Genet.* **82**, 712 (2008).
15. Materials and methods are available as supporting material on *Science* Online.
16. X. Luo, Y. Ikeda, K. L. Parker, *Cell* **77**, 481 (1994).
17. J. C. Achermann, M. Ito, M. Ito, P. C. Hindmarsh, J. L. Jameson, *Nat. Genet.* **22**, 125 (1999).
18. F. S. Alkuraya, *Genet. Med.* **12**, 236 (2010).
19. S. Harpavat, C. L. Cepko, *BMC Dev. Biol.* **6**, 2 (2006).
20. V. Anantharam, D. Zhang, L. Aravind, *Biol. Direct.* **5**, 13 (2010).
21. M. Hosokawa et al., *Dev. Biol.* **301**, 38 (2007).
22. N. Kotaja et al., *Proc. Natl. Acad. Sci. U.S.A.* **103**, 2647 (2006).
23. N. Kedersha, P. Anderson, *Methods Enzymol.* **431**, 61 (2007).
24. M. Zeitelhofer et al., *J. Neurosci.* **28**, 7555 (2008).
25. F. Roegiers, Y. N. Jan, *Trends Cell Biol.* **10**, 220 (2000).
26. L. Furic, M. Maher-Laporte, L. DesGroseillers, *RNA* **14**, 324 (2008).
27. J. P. Vessey et al., *Proc. Natl. Acad. Sci. U.S.A.* **105**, 16374 (2008).
28. Y. K. Kim, L. Furic, L. Desgroseillers, L. E. Maquat, *Cell* **120**, 195 (2005).
29. S. A. Barbee et al., *Neuron* **52**, 997 (2006).
30. M. S. Haque, J. K. Arora, G. Dikdan, T. W. Lysz, P. S. Zelenka, *Mol. Vis.* **5**, 8 (1999).
31. D. T. Gilmour et al., *EMBO J.* **17**, 1860 (1998).
32. S. A. Riazuddin et al., *Invest. Ophthalmol. Vis. Sci.* **46**, 2100 (2005).
33. N. L. Kedersha, M. Gupta, W. Li, I. Miller, P. Anderson, *J. Cell Biol.* **147**, 1431 (1999).
34. K. S. Sinsimer et al., *Mol. Cell. Biol.* **28**, 5223 (2008).
35. L. Fu, J. J. Liang, *J. Biol. Chem.* **277**, 4255 (2002).
36. L. Fu, J. J. Liang, *Biochem. Biophys. Res. Commun.* **302**, 710 (2003).
37. G. Jun et al., *PLoS Genet.* **5**, e1000584 (2009).
38. S. C. Saccà, A. Izzotti, *Prog. Brain Res.* **173**, 385 (2008).
39. This work was supported by R01 EY10123, R01 HD060050, P01 GM061354, KACST 08-MED497-20, R01 EY11721, The Barbara and Joseph Cohen Foundation, The Peace by Pieces Fund, and the Dubai Harvard Foundation for Medical Research. S.M.A. is supported by a grant from Kuwait University (YM01/09). A.V.D. was supported by a Marjorie Carr Adams Career Development Award from the Foundation Fighting Blindness. A.A. is supported by an American Heart Association Predoctoral Fellowship. S.W.M.J. and G.J.H. are Investigators of the Howard Hughes Medical Institute. We thank C. Cepko for advice on the chick experiments, L. Reinholdt for assistance in assessing male sterility, A. Bell for technical assistance, J. Reddan and V. Reddy for their gifts of lens cell lines, and the patients and their families for participating in this research. All microarray data are deposited in the Gene Expression Omnibus database (www.ncbi.nih.gov/geo), and the accession number for the SuperSeries for all data files is GSE25812.

REPORTS

Baryons at the Edge of the X-ray–Brightest Galaxy Cluster

Aurora Simionescu,[1]* Steven W. Allen,[1] Adam Mantz,[2] Norbert Werner,[1] Yoh Takei,[3] R. Glenn Morris,[1] Andrew C. Fabian,[4] Jeremy S. Sanders,[4] Paul E. J. Nulsen,[5] Matthew R. George,[6] Gregory B. Taylor[7,8]

Studies of the diffuse x-ray–emitting gas in galaxy clusters have provided powerful constraints on cosmological parameters and insights into plasma astrophysics. However, measurements of the faint cluster outskirts have become possible only recently. Using data from the Suzaku x-ray telescope, we determined an accurate, spatially resolved census of the gas, metals, and dark matter out to the edge of the Perseus Cluster. Contrary to previous results, our measurements of the cluster baryon fraction are consistent with the expected universal value at half of the virial radius. The apparent baryon fraction exceeds the cosmic mean at larger radii, suggesting a clumpy distribution of the gas, which is important for understanding the ongoing growth of clusters from the surrounding cosmic web.

Galaxy clusters provide critical constraints on cosmological parameters that are independent from those determined using type Ia supernovae, galaxy surveys, and the primordial cosmic microwave background radiation (CMB) (*1–3*). In particular, knowledge of their baryon content is a key ingredient in the use of clusters as cosmological probes (*4, 5*). Most baryons reside in the hot, diffuse, x-ray–emitting intracluster medium (ICM). Until recently, x-ray observations have generally targeted only the inner parts of clusters, where the emission is brightest, leaving a large fraction of their volumes practically unexplored. Estimates of the gas mass and total mass at large radii have relied on simple model extrapolations of the thermodynamic properties measured at smaller radii.

X-ray spectroscopy of the outer regions of galaxy clusters was made possible only recently, with the use of the Suzaku satellite. Because of its much lower instrumental background than that of other x-ray observatories, Suzaku can measure the characteristics of the faint emission from cluster outskirts more reliably. Even so, few such observations have been published, and the thermodynamic profiles at large radii are not well resolved (*6–11*). The Perseus Cluster of galaxies is the brightest extragalactic extended x-ray source. It is a relaxed system, both closer (at a redshift of 0.0183) and substantially brighter than any of the other clusters for which Suzaku has previously been used to study the ICM properties at large radii. Its large angular size mitigates the impact of residual systematic uncertainties in modeling the effects of Suzaku's complex point-spread function (PSF), making the Perseus Cluster an ideal target in which to study cluster outskirts.

A large mosaic of Suzaku observations of the Perseus Cluster, with a total exposure time

[1]Kavli Institute for Particle Astrophysics and Cosmology, Stanford University, 452 Lomita Mall, Stanford, CA 94305, USA. [2]NASA Goddard Space Flight Center, Greenbelt, MD 20771, USA. [3]Institute of Space and Astronautical Science, Japan Aerospace Exploration Agency (JAXA), 3-1-1 Yoshinodai, Sagamihara, Kanagawa 229-8510, Japan. [4]Institute of Astronomy, Madingley Road, Cambridge CB3 0HA, UK. [5]Harvard-Smithsonian Center for Astrophysics, 60 Garden Street, Cambridge, MA 02138, USA. [6]Department of Astronomy, University of California, Berkeley, CA 94720, USA. [7]Department of Physics and Astronomy, University of New Mexico, Alberquerque, NM 87131, USA. [8]National Radio Astronomy Observatory, 1003 Lopezville Rd., Socorro, NM 87801, USA.

*To whom correspondence should be addressed. E-mail: asimi@stanford.edu